Model-independent periodic stability analysis of wind turbines

C.L. Bottasso[1,2] and S. Cacciola[1]

[1] Wind Energy Institute, Technische Universität München, Garching bei München, Germany
[2] Dipartimento di Scienze e Tecnologie Aerospaziali, Politecnico di Milano, Milan, Italy

Correspondence
C.L. Bottasso, Wind Energy Institute, Technische Universität München, Boltzmannstraße 15, D-85748 Garching bei München, Germany.
E-mail: carlo.bottasso@tum.de

Received 6 September 2012; Revised 4 December 2013; Accepted 12 February 2014

1. INTRODUCTION AND MOTIVATION

The estimation of damping is useful in a variety of tasks related to the design and verification of a wind turbine, for example, for explaining the causes of observed vibration phenomena, for assessing the proximity of the flutter boundaries to the operating envelope of the machine and for evaluating the efficacy of control laws in increasing the damping of low-damped modes. It is expected that the design of the future large and very large wind turbines that are being proposed for the exploitation of off-shore resources will further increase the importance of stability analysis. In fact, new designs will explore rotors of low solidity with long, slender and light-weight blades operating at high tip-speed-ratios, whose response will be affected not only by the drive-train/nacelle/tower flexibility but also by the additional couplings induced by the hydro-elastic characteristics of the submerged, and possibly floating, structure and by its interaction with the marine environment.

Linear stability analysis methods use some appropriate linear models of the system, capable of representing with sufficient fidelity its response in the proximity of a given operating condition. If the model is assumed to be linear time invariant (LTI), then stability can be readily assessed by LTI stability theory, for which a variety of methods is readily available.[1–5]

However, wind turbine models are more appropriately characterized by *periodic* rather than time invariant coefficients.[6] In fact, periodic effects are caused by gravitational and aerodynamic loads, the latter due to rotor-in-plane wind components, vertical and horizontal wind shears, and the interaction with the tower. Therefore, linear time periodic (LTP) models, whose stability characteristics are described by the Floquet theory,[7] are customarily employed.

Rather than directly applying the Floquet theory on an LTP model to study its stability, one can first turn the LTP model into an equivalent LTI one by a coordinate transformation and then perform a standard LTI stability analysis. The infinitely numerous Lyapunov–Floquet coordinate transformations make this possible by achieving the exact cancelation of all periodic effects from the model. However, a more common approach[8,9] is to use the multi-blade coordinate (MBC) transformation of Coleman and Feingold[10,11] (cf. also the review given by Bir[12]). This transformation, which can be interpreted as an approximation of one of the exact Lyapunov–Floquet transformations,[9,13] expresses the model rotating degrees of freedom into an inertial frame with the effect of a strong reduction, but in general not an exact elimination, of the periodic content of the state matrix. In fact, only in the case of a perfectly isotropic rotor (with identical blades, uniform wind and in the absence of gravity) is the multi-blade transformation equal to one of the Floquet–Lyapunov transformations and performs a perfect cancelation of the periodic terms. The periodicity that remains in the general case after the application of the multi-blade transformation is either neglected or removed by averaging, so that the resulting LTI model can at this point be analyzed using standard invariant techniques. We will call this approach in the following *MBC-LTI*. The neglected periodicity is more relevant for anisotropic rotors (i.e., when blades are aerodynamically or structurally different), for anisotropic wind conditions (i.e., with shears and/or cross-flow) and in the presence of gravity; the effects of such approximations on the stability analysis, although often acceptable in many cases, are, however, in general difficult to assess and quantify *a priori*.

This discussion highlights the fact that there are two main aspects in the stability analysis of wind turbines: periodicity and the dependence on a model. This paper proposes a new approach that accounts for both in ways that try to overcome some limitations of current methods.

1.1. Periodicity

Regarding periodicity, we develop a method that rigorously accounts for the periodic nature of the problem, building on the Floquet stability theory of LTP systems.[14,15] The motivation behind this approach lies in the fact that the approximate treatment of periodic terms of contemporary methods implies approximations that invariably neglect some aspects of the behavior of the system. Although such approximations may have been usually acceptable for the current wind turbines, they may become more questionable as industry explores designs of increasing size that try to beat the cubic weight growth curve, as highlighted in Section 2.3.

In fact, periodic stability theory shows a richer picture than the one customarily obtained by the use of the standard approximate transformation methods described earlier, as first noticed by Bottasso and Cacciola.[16] For each of the harmonics computed by the MBC-LTI approach (e.g., first tower fore-aft, first blade flap, first blade edge and second blade flap), the fully periodic approach reveals the presence of a *fan* made by an infinite number of harmonics of varying 'strength'.

To better illustrate this concept, Figure 1 shows at the left a Campbell diagram obtained by the MBC-LTI approach and at the right its fully periodic version. As customarily carried out, the plot represents the system harmonics ω vs. the rotor speed Ω; the plot also reports the per-rev excitation harmonics indicated as straight dashed lines emanating from the origin. For simplicity of exposition, and not to clutter the figure, the plot on the left shows only one single frequency, which by its shape and location in this qualitative image might represent the first flap blade frequency, slightly increasing with respect to the rotor speed due to centrifugal stiffening. The left part of the figure is the Cambell diagram representation that would normally be obtained by using a classical approach, and which represents an important design tool since it readily illustrates the possible intersections between system eigenfrequencies and per-rev excitation harmonics.

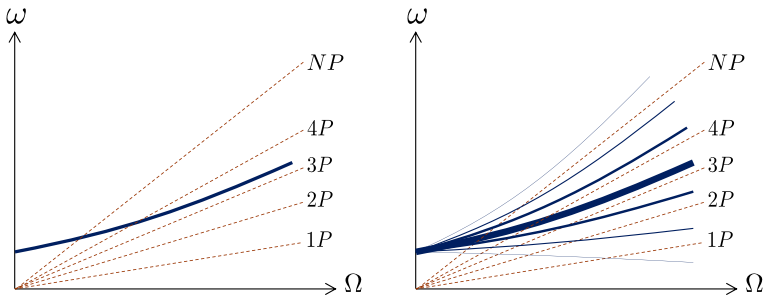

(a) MBC-LTI (b) LTP

Figure 1. Qualitative standard (left) and periodic (right) Campbell diagrams (for clarity, one single mode is shown for the standard diagram, and the corresponding single fan for the periodic one).

In reality, a rigorous LTP analysis reveals the picture shown on the right part of Figure 1. Here, for that same first blade flap mode, we observe not only the principal harmonic already visible in the left plot but also an infinite number of associated *super-harmonics* fanning out from the principal one at $\pm k\Omega$, $k = 1, \ldots, \infty$. All harmonics in the fan have a varying degree of 'strength', indicated in the picture by the thickness of the solid line. These additional super-harmonics are invisible to the classical approach.*

These results descend directly from the theory of periodic systems, which shows that the contractivity of the solution is contained in the monodromy matrix, i.e., the matrix mapping the system states into the states after one period (one rotor revolution). By spectral decomposition of the monodromy matrix, the characteristic multipliers are obtained, from which one can readily derive the characteristic exponents. In turn, the characteristic exponents, being the analogues of the eigenvalues in the LTI case, yield the frequency and damping factor of each harmonic of the system. Finally, the periodic eigenvectors of the system are computed, which yield *modal participation factors* that measure the relative strength of each harmonic within its fan, as illustrated in the plot in Figure 1 and explained in detail in Section 2.1. Modal participation factors rigorously clarify the degree of periodicity of each fan. In fact, the closer the participation of a certain harmonic is to 1, the more that fan behaves as invariant (i.e., non-periodic); in the limit, if one harmonic has a participation factor of exactly 1 and all others are 0, then the fan collapses into a single line, yielding the usual picture seen at the left in Figure 1. On the other hand, if some super-harmonics have significant participation factors, then the fan is strongly affected by periodicity. In such cases, crossing of a significant super-harmonic with a per-rev excitation in conditions where enough energy is present (e.g., high rotor speeds) may result in vibratory phenomena;[13] such situations would not be explainable if one tried to describe a mode of an LTP system with a single frequency as in the LTI case. The MBC-LTI analysis of a three-bladed rotor detects the two lower super-harmonics, i.e., the ones separated from the principal one by $+\Omega$ and $-\Omega$ (see the work of Skjoldan and Hansen[13] and Hansen[17,18]), while all other higher super-harmonics will be missed by such an approach. Within the MBC-LTI method, these two super-harmonics are usually called backward and forward whirling components,[18] a somewhat misleading name that might create confusion with the whirling modes generated by the coupling between rotor blade deflections and the flexible support structure.

1.2. Model independence

Regarding the dependence on a model for the conduction of a stability analysis, we remark that methods that rely on coordinate transformations, such as the MBC-LTI approach described earlier, are usually difficult to implement and maintain. In fact, given the software implementation of any suitable mathematical wind turbine model, one would first have to develop its linearization. Next, one would need to implement the Coleman transformation of the rotating degrees of freedom of the model, followed by some specific additional elaboration to remove any remaining periodic term. It is clear that, if the original non-linear model is of high fidelity and hence highly complex, as the ones used in most current comprehensive codes, then the implementation of these software modifications can imply a considerable effort. Even more importantly, it means that every time the non-linear model is improved or expanded, this has to be followed by a similar upgrade of its MBC-LTI derivation.

To overcome such hurdles, in this work, periodic stability analysis theory is not applied to the analytical expression of a specific model, but rather it is formulated in terms of input–output discrete-time histories. Such time histories could come from 'virtual' experiments performed on any model, from simplified ones to the more advanced contemporary comprehensive multibody-based aero-hydro-servo-elastic models. On the practical side, this implies that one can easily replace the model with a different (new or better) one, without having to modify or adjust in any way the stability analysis procedure. Furthermore, by properly expanding the formulation presented here to include the effects of process noise and to consider the presence of a closed-loop controller, the time histories could also come from measurements obtained on the real wind turbine operating in the field.

Using this approach, inputs are represented by either pitch, torque, wind and/or externally applied force signals, studied so as to excite the response of the mode(s) of interest. On the other hand, outputs are represented by the corresponding measurements of components of the system response (velocities, accelerations, loads, etc.), chosen so as to exhibit a high informational content on the mode(s) of interest. This procedure is graphically depicted in Figure 2.

Given such suitable input–output time histories, a Periodic Auto-Regressive model with eXogenous inputs (PARX)[19] is fitted to the histories using system identification techniques, and more specifically with the output-error method.[20,21] Finally, the periodic stability analysis theory of Floquet is applied to the state-space realization of the identified model to yield frequencies, damping and modal participation factors of each harmonic in each fan. From this point of view, this

*The LTP theory does not allow for the classification of one specific harmonic as the principal one, as the whole fan of harmonics is generated as part of the analysis. However, to ease the bridge between the classical view and the present one, we term here and in the following 'principal harmonic' the member of the fan that most closely resembles the one that would have been obtained by the MBC-LTI approach; coherently, all other members of the same fan are termed 'super-harmonics'.

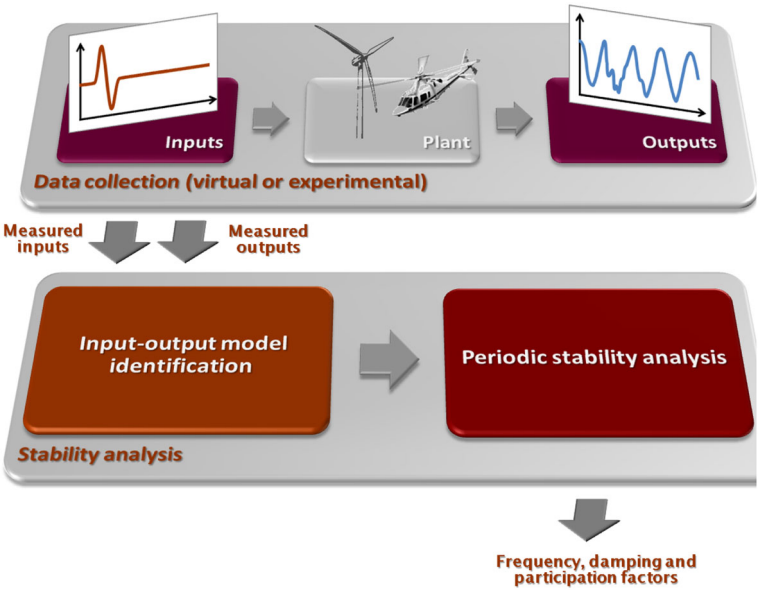

Figure 2. Model-independent stability analysis process.

method could be interpreted as an extension to periodic models of the method of Prony.[22] A somewhat related approach is pursued by Allen *et al.*,[23] which proposes an output-only modal analysis in the frequency domain, made possible by the identification of the periodic harmonic transfer function of the system.[14]

1.3. Organization of the paper

The paper is organized according to the following plan.

At first, the stability theory of LTP systems is briefly reviewed in Section 2. The continuous and discrete-time formulations described in Sections 2.1 and 2.2 explain the presence of the frequency fans and lead to the definition of the modal participation factors as periodicity indicators. To better illustrate these concepts, we consider in Section 2.3 the simplified model problem of a rotor-tower system *in vacuo*, which also clearly establishes the differences between a periodic stability analysis and an approximate MBC-LTI one.

Next, Section 3 describes the process of identifying LTP systems from input–output data. The equation-error approach, used to initialize the solution, is formulated in Section 3.1, while the output-error method, used to actually compute the solution, in Section 3.2. Finally, Section 3.3 describes the realization of the identified periodic reduced model in state-space form.

The paper is completed by several numerical experiments, reported in Section 4, which illustrate the main findings of this work with the help of the detailed model of a multi-MW wind turbine implemented in a high-fidelity aero-servo-elastic simulation code.

2. STABILITY ANALYSIS OF LTP SYSTEMS

2.1. Continuous time

A generic LTP system in continuous time can be written in state-space form as

$$\dot{\boldsymbol{x}} = \boldsymbol{A}(t)\boldsymbol{x} + \boldsymbol{B}(t)\boldsymbol{u} \tag{1a}$$

$$y = \boldsymbol{C}(t)\boldsymbol{x} + \boldsymbol{D}(t)\boldsymbol{u} \tag{1b}$$

where t is time, $\boldsymbol{x}$ and $\boldsymbol{u}$ are the state and input vectors, respectively, y is a scalar output, while $\boldsymbol{A}(t)$, $\boldsymbol{B}(t)$, $\boldsymbol{C}(t)$ and $\boldsymbol{D}(t)$ are periodic system matrices such that

$$\boldsymbol{A}(t+T) = \boldsymbol{A}(t), \quad \boldsymbol{B}(t+T) = \boldsymbol{B}(t) \tag{2a}$$

$$\boldsymbol{C}(t+T) = \boldsymbol{C}(t), \quad \boldsymbol{D}(t+T) = \boldsymbol{D}(t) \tag{2b}$$

for each t. The smallest T satisfying equation (2) is defined as the system period. Vector $\boldsymbol{u}$ contains the machine control inputs (i.e., blade pitch angles, electrical torque and possibly the yaw angle) as well as exogenous inputs related to the wind states (e.g., wind speed, vertical or lateral shears, and cross-flow). The closed-loop case may be considered by including the effects of the control law in the $\boldsymbol{A}(t)$ matrix; in this case, the $\boldsymbol{u}$ vector is only related to wind states.

To study the stability of (1a), its autonomous version is considered together with associated initial conditions:

$$\dot{\boldsymbol{x}} = \boldsymbol{A}(t)\boldsymbol{x}, \quad \boldsymbol{x}(0) = \boldsymbol{x}_0. \tag{3}$$

The state transition matrix $\Phi(t)$, which maps the initial state $\boldsymbol{x}_0$ into the state $\boldsymbol{x}(t)$ at time t through

$$\boldsymbol{x}(t) = \Phi(t)\boldsymbol{x}_0. \tag{4}$$

obeys a similar equation with its initial conditions:

$$\dot{\Phi}(t) = \boldsymbol{A}(t)\Phi(t), \quad \Phi(0) = \boldsymbol{I} \tag{5}$$

where $\boldsymbol{I}$ is the identity matrix.

According to the Floquet theory,[7] Φ can be decomposed as

$$\Phi(t) = \boldsymbol{P}(t)e^{\boldsymbol{R}\,t}, \quad \boldsymbol{P}(0) = \boldsymbol{I} \tag{6}$$

where the first term $\boldsymbol{P}(t) = \boldsymbol{P}(t+T)$ is the *periodic eigenvector*, while the second captures the contractivity of the solution, $\boldsymbol{R}$ being a constant matrix termed *Floquet factor*. For a given $\boldsymbol{R}$, $\boldsymbol{P}(t)$ can be readily computed from (9) as

$$\boldsymbol{P}(t) = \Phi(t)e^{-\boldsymbol{R}\,t}. \tag{7}$$

The periodic eigenvector $\boldsymbol{P}(t)$ can be used to perform a change of coordinates that transforms the LTP system into an invariant one. In fact, by choosing a variable $\boldsymbol{v}(t) = \boldsymbol{P}(t)^{-1}\boldsymbol{x}(t)$, the autonomous system (3) becomes LTI:

$$\dot{\boldsymbol{v}}(t) = \boldsymbol{R}\boldsymbol{v}(t). \tag{8}$$

The state transition matrix over one period,

$$\Psi = \Phi(T) = e^{\boldsymbol{R}\,T} \tag{9}$$

is termed *monodromy matrix*. The eigenvalues θ_j and associated eigenvectors $\boldsymbol{s}_j$, $j = 1, \ldots, N_s$, N_s being the number of states in the system, are obtained by spectral factorization of the monodromy matrix,

$$\Psi = \boldsymbol{S}\,\mathrm{diag}\{\theta_j\}\,\boldsymbol{S}^{-1} \tag{10}$$

with $\boldsymbol{S} = [\ldots, \boldsymbol{s}_j, \ldots]$. System (3) is asymptotically stable if and only if the eigenvalues θ_j, termed *characteristic multipliers*, belong to the open unit disk in the complex plane. From the factorization of Ψ, recalling (9), one obtains the factorization of $\boldsymbol{R}$ as

$$\boldsymbol{R} = \boldsymbol{S}\,\mathrm{diag}\{\eta_j\}\,\boldsymbol{S}^{-1} \tag{11}$$

where the *characteristic exponents* η_j are related to the characteristic multiplies θ_j through the following expression:

$$\theta_j = e^{\eta_j T}. \tag{12}$$

Apparently, computing the characteristic exponents from the characteristic multipliers by equation (12) leads to a multiplicity of solutions, as

$$\eta_j = \frac{1}{T}\log\theta_j = \frac{1}{T}\left(\log|\theta_j| + i(\angle(\theta_j) + 2\ell\pi)\right) \tag{13}$$

where $\ell \in \mathbb{Z}$ is an arbitrary integer. This indeterminacy, however, does not, and cannot for clear physical reasons, affect the real frequency content of the response, as explained here in the following and as first observed by Borri[24] and later discussed by Peters *et al.*[15]

Inserting (11) into (6), one can express the state transition matrix as

$$\Phi(t) = \sum_{j=1}^{N_s} \boldsymbol{Z}_j(t) e^{\eta_j t} \tag{14}$$

where $\boldsymbol{Z}_j(t) = \boldsymbol{P}(t)\boldsymbol{S}\boldsymbol{I}_{jj}\boldsymbol{S}^{-1}$, while $\boldsymbol{I}_{jj}$ is a matrix with the sole element (j, j) equal to 1 and all others equal to 0. Since $\boldsymbol{Z}_j(t)$ is a periodic matrix, it can be expanded in a Fourier series as follows:

$$\boldsymbol{Z}_j(t) = \sum_{n=-\infty}^{+\infty} \boldsymbol{Z}_{j_n} e^{i n \frac{2\pi}{T} t} \tag{15}$$

where $\boldsymbol{Z}_{j_n}$ is the matrix of complex amplitudes of the nth harmonic of $\boldsymbol{Z}_j(t)$. By combining now equation (14) with (15), the following expression for the transition matrix is derived:

$$\Phi(t) = \sum_{j=1}^{N_s} \sum_{n=-\infty}^{+\infty} \boldsymbol{Z}_{j_n} e^{(\eta_j + i n \frac{2\pi}{T})t}. \tag{16}$$

For the LTP problem, the exponents $\eta_j + i n 2\pi/T$ play the role of the eigenvalues of the LTI case, as they yield the frequencies $\omega_{j_n} = |\eta_j + i n 2\pi/T|$ and the damping factors $\xi_{j_n} = -\mathrm{Re}(\eta_j)/\omega_{j_n}$ of each mode of the system. However, in marked contrast with the LTI case where for each state there is a single mode at a single frequency, in the LTP case for each state j in (16) there is an infinite number of frequencies that participate in the response of the system. To describe this situation, we propose to term a fan of modes each infinite multiple of frequencies (and their associated shapes) characterized by the same characteristic exponent η_j and by varying imaginary exponents $i n 2\pi/T$.

Each mode in a fan contributes to the overall response according to its associated 'modal shape' $\boldsymbol{Z}_{j_n}$. In order to quantify the relative contribution to the response of each harmonic $\eta_j + i n \frac{2\pi}{T}$, its *participation factor* can be defined as

$$\phi_{j_n} = \frac{\|\boldsymbol{Z}_{j_n}\|}{\sum_n \|\boldsymbol{Z}_{j_n}\|} \tag{17}$$

where $\|\cdot\|$ is a matrix norm, chosen here as the Frobenius one.

If all Fourier coefficients of $\boldsymbol{Z}_j$ in equation (15) were equal to 0, except for one related to a certain harmonic, then the periodic transition matrix (16) would result in the standard invariant transition matrix; the only surviving harmonic would have a participation factor exactly equal to one. This fact suggests the use of the harmonic participation factor as a 'periodicity indicator': the closer the participation of a certain harmonic of a given mode is to one, the more that mode behaves as invariant.

Participation factors not only play the role of periodicity indicators but also clarify the apparent indeterminacy in the computation of the imaginary part of the logarithm of the characteristic multipliers in equation (13). This indetermination does not have any practical effect if one computes also the periodic eigenvectors and their participation factors. In fact, all theoretically infinite exponents $\eta_j + i 2n\pi/T$ in (16) satisfy equation (12), so that the ambiguity in their imaginary part is only apparent. Since the transition matrix remains uniquely defined, any choice of the arbitrary integer ℓ (for example, $\ell = 0$) coherently affects the harmonic content of the periodic eigenvectors $\boldsymbol{P}(t)$, such that the harmonics involved in the response of the system remain exactly the same and with the same participation factors.[15,24] This implies that triads ω_{j_n}, ξ_{j_n} and ϕ_{j_n} remain uniquely defined.

Often, although not always, the harmonic with the highest participation is very similar in terms of frequency and damping to the one that would result from an MBC-LTI approach. As previously noted, such harmonic may be called the principal one, while the others may be termed super-harmonics. The formulas, however, show clearly that such a dichotomy, although useful to bridge the classical and periodic views, is in reality wrong, since periodic modes are not defined by a single frequency but by an infinite multitude, where each frequency is spaced from its two neighbors by plus and minus the rotor speed $\Omega = 2\pi/T$. Furthermore, any one of these harmonics could resonate with the external excitations.

Output-specific participation factors can be defined as well. This can be useful because, as it will be shown later on, a mode may behave more or less periodically with respect to different outputs. In the case of a constant output matrix $\boldsymbol{C}(t) = \boldsymbol{C}$, to measure the participation to a given output y, an output-specific participation factor can be defined as

$$\phi_{j_n}^{y} = \frac{\|\boldsymbol{C}\boldsymbol{Z}_{j_n}\|}{\sum_n \|\boldsymbol{C}\boldsymbol{Z}_{j_n}\|}. \tag{18}$$

The case of a periodic output matrix $\boldsymbol{C}(t)$ is of particular interest because different periodic output matrices can describe how different observers, located, for example, in rotating or fixed frames of reference, sense the dynamics of rotors. Consider a generic periodic output equation with no inputs, $\boldsymbol{y}(t) = \boldsymbol{C}(t)\boldsymbol{x}(t)$. By using the state transition matrix, the output is computed as

$$\boldsymbol{y}(t) = \Phi_y(t)\boldsymbol{x}(0) = \boldsymbol{C}(t)\Phi(t)\boldsymbol{x}(0) \tag{19}$$

and consequently

$$\Phi_y(t) = \boldsymbol{C}(t)\sum_{j=1}^{N_s}\sum_{n=-\infty}^{\infty}\boldsymbol{Z}_{j_n}e^{(\eta_j+in\frac{2\pi}{T})t}. \tag{20}$$

By expanding $\boldsymbol{C}(t)$ into a Fourier series as

$$\boldsymbol{C}(t) = \sum_{m=-\infty}^{\infty}\boldsymbol{C}_m e^{im\frac{2\pi}{T}t} \tag{21}$$

and inserting into (20), one obtains

$$\Phi_y(t) = \sum_{j=1}^{N_s}\sum_{m=-\infty}^{\infty}\sum_{n=-\infty}^{\infty}\boldsymbol{C}_m\boldsymbol{Z}_{j_n}e^{(\eta_j+i(n+m)\frac{2\pi}{T})t}. \tag{22}$$

Introducing index $r = n + m$, one finally obtains

$$\Phi_y(t) = \sum_{j=1}^{N_s}\sum_{r=-\infty}^{\infty}\boldsymbol{G}_{j_r}e^{(\eta_j+ir\frac{2\pi}{T})t}. \tag{23}$$

where

$$\boldsymbol{G}_{j_r} = \sum_{m=-\infty}^{\infty}\boldsymbol{C}_m\boldsymbol{Z}_{j_{r-m}}. \tag{24}$$

By using (23) and (24), the output-specific participation factor is defined in this case as

$$\phi^y_{j\,r} = \frac{\|\boldsymbol{G}_{j_r}\|}{\sum_r\|\boldsymbol{G}_{j_r}\|}. \tag{25}$$

It should be noticed that a periodic output matrix does not modify the fan of frequencies belonging to a certain mode; in fact, as expected, the characteristic exponents remain unaffected, and only the related participations change. Now, recalling that a change of observation frame, e.g., from the fixed to the rotating one, can be obtained by the use of a suitable periodic output matrix $\boldsymbol{C}(t)$, it follows that the frequency content of a rotor is *independent* from the frame of reference. In light of the Floquet theory, the dualism 'fixed/rotating frame frequencies', although widely accepted and often used in practice, is in reality not correct; this fact will be better explained with the help of a model problem in Section 2.3. On the other hand, as shown by (24) and (25), the participation of a certain harmonic may appear more or less prominently if viewed from different observation frames.

2.2. Discrete time

The autonomous dynamic equations of a generic LTP system in discrete time and their initial conditions are

$$\boldsymbol{x}(k+1) = \boldsymbol{A}(k)\boldsymbol{x}(k), \quad \boldsymbol{x}(0) = \boldsymbol{x}_0 \tag{26}$$

where k is a generic time instant and $\boldsymbol{A}(k)$ is a periodic matrix of period K such that $\boldsymbol{A}(k+K) = \boldsymbol{A}(k)\ \forall k$. Similarly, the transition matrix obeys the following equations and initial conditions:

$$\Phi(k+1) = \boldsymbol{A}(k)\Phi(k), \quad \Phi(0) = \boldsymbol{I}. \tag{27}$$

In this work, we consider only reversible discrete-time systems, i.e., those for which $\det(\Phi(k)) \neq 0\ \forall k$, while reversibility is always guaranteed in the continuous-time case (cf. Bittanti and Colaneri[14] for a general treatment).

For reversible discrete-time systems, the state transition matrix $\Phi(k)$ can be decomposed in periodic and contractive factors as

$$\Phi(k) = \boldsymbol{P}(k)\boldsymbol{R}^k \tag{28}$$

where $\boldsymbol{P}(k)$ is periodic and $\boldsymbol{R}$ is constant. Here again, the monodromy matrix is defined as the transition matrix over one period, i.e.,

$$\Psi = \Phi(K) = \boldsymbol{R}^K \tag{29}$$

whose spectral decomposition yields its characteristic multipliers θ_j and eigenvectors $\boldsymbol{S}$:

$$\Psi = \boldsymbol{S}\,\mathrm{diag}\{\theta_j\}\,\boldsymbol{S}^{-1}. \tag{30}$$

The relationship between characteristic multipliers and characteristic exponents becomes then

$$\boldsymbol{\theta}_j = \boldsymbol{\eta}_j^K. \tag{31}$$

In the discrete-time case, the apparent multiplicity of the characteristic exponents appears as a phase indetermination, since

$$\eta_j = \sqrt[K]{|\theta_j|}\left(\cos\left(\frac{\angle(\theta_j)+2\ell\pi}{K}\right)+i\sin\left(\frac{\angle(\theta_j)+2\ell\pi}{K}\right)\right) \tag{32}$$

where $\ell = 0, \ldots, K-1$ is an arbitrary integer. As in the continuous-time case, this does not in reality generate any inconsistency since frequencies, damping and participation factors of the various harmonics are unaffected by this apparent arbitrariness.

Following the same approach of the continuous-time case, the transition matrix can be written as

$$\Phi(t) = \sum_{j=1}^{N_s}\sum_{n=0}^{K-1}\boldsymbol{Z}_{j_n}\left(|\eta_j|e^{(i\angle(\eta_j)+n\frac{2\pi}{K})}\right)^k. \tag{33}$$

This shows that the jth mode is characterized by K exponents with the same modulus and different phases. Each exponent can be transformed into the continuous one using the following expression (cf. Franklin and Powell,[25] p. 31)

$$\eta_{j_c} = \frac{1}{\Delta t}\log(\eta_{j_d}) \tag{34}$$

where Δt is the sampling time and subscripts $(\cdot)_c$ and $(\cdot)_d$ refer, respectively, to the continuous and discrete-time cases. Once the continuous-time exponents are computed, frequencies, damping and participation factors can be readily obtained.

2.3. Illustration by a model problem

A simple model problem is used for illustrating the main characteristics of the periodic stability analysis described earlier. The problem represents the coupled side–side tower and edgewise blade response of a wind turbine *in vacuo*. In this simplified model, the side–side flexibility of the tower is rendered by an equivalent spring that connects the hub to the ground.[26] Similarly, the blade is represented by a rigid body connected to the hub by means of an equivalent hinge, whose characteristics in terms of offset from the axis of rotation and stiffness are chosen so as to match the first edgewise natural frequency of the blade.[6] As gravity is included in the model, the blade stiffness varies periodically under the effects of its own weight, effects that depend on the blade azimuthal position in its travel around the rotor disk. Figure 3 shows a sketch of the system, whereas Table I reports a list of the main model parameters and their values.

The $B+1$ linearized periodic equations of motion of the system write

$$\boldsymbol{M}(\quad)\ddot{\boldsymbol{q}}(t) + \boldsymbol{C}(\psi)\dot{\boldsymbol{q}}(t) + \boldsymbol{K}(\psi)\boldsymbol{q}(t) = 0 \tag{35}$$

where vector of coordinates $\boldsymbol{q}$ is defined as

$$\boldsymbol{q}(t) = (\zeta_1(t), \zeta_2(t), \zeta_3(t), y_c(t))^T. \tag{36}$$

ζ_i is the lag angle of the ith blade, and y_c the horizontal displacement of the hub, while the azimuthal angles of the rotor and of the individual blades are indicated respectively with $\psi = \psi_1 = \Omega(t)t$ and $\psi_i = \psi_1 + (i-1)2\pi/B$, $i = 2, 3$; finally, the mass, damping and stiffness matrices write

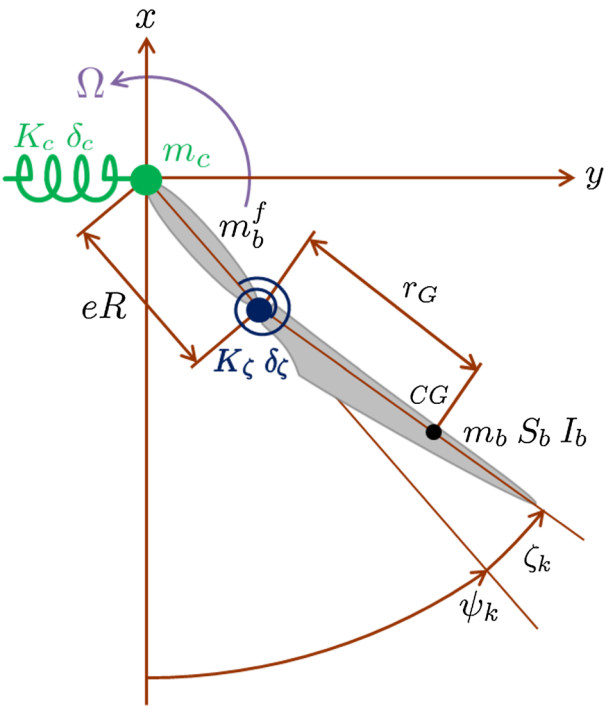

Figure 3. Schematic view of the rotor-tower model system. Only one blade is shown, for clarity.

Table I. Rotor-tower model system: main parameters and their numerical values.

Parameter	Symbol	Value	
Number of blades	B	3	
Rotor radius	R	75	(m)
Rated rotor speed	Ω_r	1.2	(rad s^{-1})
Hinge offset	e	25.651	(%R)
Mass of hub	m_h	7.5000E+4	(kg)
Blade mass (movable part)	m_b	1.4482E+4	(kg)
Blade mass (fixed part)	m_b^f	1.0873E+4	(kg)
Blade static moment	S_b	2.7116E+5	(kg m)
Blade moment of inertia	I_b	7.4881E+6	(kg m^2)
Edgewise spring stiffness	K_ζ	2.1192E+8	(N m)
Edgewise spring damper	δ_c	1.7555E+6	(N m s)
Tower spring stiffness	K_c	7.3116E+5	(N m^{-1})
Tower spring damper	δ_c	1.3294E+4	(N s m^{-1})

$$\boldsymbol{M}(\ ) = \begin{bmatrix} I_b & 0 & 0 & S_b\sin(\psi_1) \\ 0 & I_b & 0 & S_b\sin(\psi_2) \\ 0 & 0 & I_b & S_b\sin(\psi_3) \\ S_b\sin(\psi_1) & S_b\sin(\psi_2) & S_b\sin(\psi_3) & m_h + B\left(m_b + m_b^f\right) \end{bmatrix} \tag{37a}$$

$$\boldsymbol{C}(\ ) = \begin{bmatrix} \delta_b & 0 & 0 & 0 \\ 0 & \delta_b & 0 & 0 \\ 0 & 0 & \delta_b & 0 \\ -2S_b\Omega\sin(\psi_1) & -2S_b\Omega\sin(\psi_2) & -2S_b\Omega\sin(\psi_3) & \delta_c \end{bmatrix} \tag{37b}$$

Table II. Frequency in hertz of the harmonics with the five highest participation factors at rated rotor speed, grouped by classical modes.

	Tower	Backward whirl	Blade edgewise	Forward whirl
Super-harmonic ($-i2\Omega$)	0.0378	0.3036	0.4649	0.6823
Super-harmonic ($-i\Omega$)	0.1533	0.4940	0.6558	0.8731
Principal harmonic	0.3443	0.6847	0.8467	1.0640
Super-harmonic ($+i\Omega$)	0.5352	0.8756	1.0377	1.2549
Super-harmonic ($+i2\Omega$)	0.7262	1.0665	1.2286	1.4458

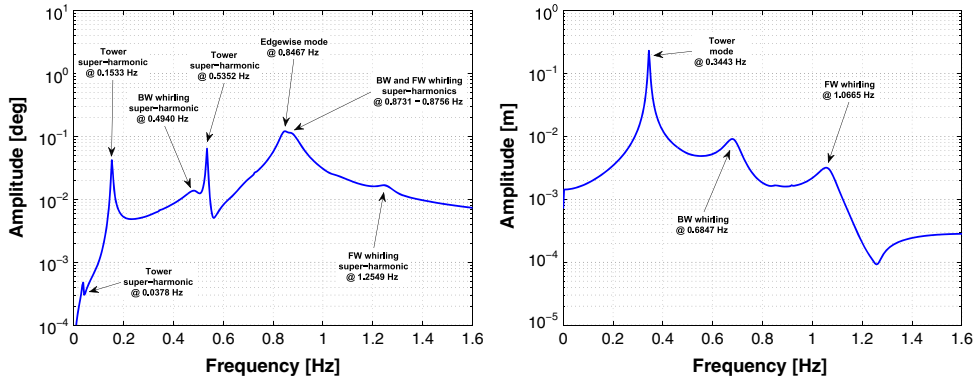

(a) Blade response (b) Tower response

Figure 4. Fast Fourier transform of the transient response of the rotor-tower model problem.

Table III. Output-specific participation factors for the frequencies of Table II.

	Tower		Backward whirl		Blade edgewise		Forward whirl	
	ζ_1	y_C	ζ_1	y_C	ζ_1	y_C	ζ_1	y_C
Super-harmonic ($-i2\Omega$)	0.0024	0.0000	0.0007	0.0001	0.0001	0.0006	0.0138	0.0012
Super-harmonic ($-i\Omega$)	0.3763	0.0000	0.0980	0.0001	0.0111	0.0025	0.9186	0.0000
Principal harmonic	0.0017	0.9997	0.0173	0.9940	0.9725	0.9682	0.0095	0.9339
Super-harmonic ($+i\Omega$)	0.6058	0.0000	0.8719	0.0001	0.0158	0.0012	0.0561	0.0001
Super-harmonic ($+i2\Omega$)	0.0120	0.0000	0.0111	0.0002	0.0001	0.0002	0.0002	0.0000

$$\boldsymbol{K}(\ \ ) = \begin{bmatrix} K_\zeta + eR\Omega^2 + g\,S_b\cos(\psi_1) & 0 & 0 & 0 \\ 0 & K_\zeta + eR\Omega^2 + g\,S_b\cos(\psi_2) & 0 & 0 \\ 0 & 0 & K_\zeta + eR\Omega^2 + g\,S_b\cos(\psi_3) & 0 \\ -S_b\Omega^2\cos(\psi_1) & -S_b\Omega^2\cos(\psi_2) & -S_b\Omega^2\cos(\psi_3) & K_c \end{bmatrix}. \tag{37c}$$

A classical MBC-LTI analysis would lead to the identification of four modes, which include the tower side–side, backward in-plane whirling, blade edgewise and forward in-plane whirling modes, in the order from lower to higher frequencies. A time continuous periodic stability analysis was performed from varying rotor speeds, which, as previously discussed, reveals a much higher number of harmonics. To illustrate this fact, the frequencies of the harmonics with the five highest participation factors are reported in Table II for the rated rotor speed case; these frequencies were grouped according to the principal classical modes named earlier.

Figure 4 shows the response spectra of one of the blades, at the left, and the hub, at the right. By comparing these spectra with Table II, one can easily identify most frequencies. In particular, a part from the well-known principal harmonics, one should notice the two tower super-harmonics that appear very prominently in the blade response spectrum at 0.1533 and 0.5352 Hz. These frequencies would be missed if one tried to describe a periodic mode with a single frequency.

Table III illustrates the fact that each fan of modes may exhibit a more or less periodic behavior when looking at specific outputs. For each frequency of Table II, the table reports the participation factors of output ζ_1 (at the left) and output y_c (at the right), computed using (18) with $\boldsymbol{C}$ equal to [1 0 0 0] and [0 0 0 1], respectively. For example, the tower fan of modes

behaves as largely invariant when observed through the tower displacement y_c (cf. the principal harmonic participation at 0.9997) but has a strongly periodic character when observed through the blade lag response (cf. the principal harmonic participation at 0.0017, while the super-harmonics $+i\Omega$ and $-i\Omega$ are 0.6058 and 0.3763, respectively). A similar behavior is observed for the backward and forward in-plane whirls, while the opposite is true for the blade edgewise one. These non-classical effects stress further the difference between the LTI and LTP views of the problem, the latter being much more complex and richer than the former. This also highlights once more the arbitrariness of labeling a frequency as the principal harmonic: what appears prominently in one output (e.g., the 'classical' tower frequency in the tower displacement) can almost disappear in comparison with its super-harmonics in another output (e.g., again the 'classical' tower frequency observed in the blade lag response). Nonetheless, we keep using this terminology in the following for its practical utility and to ease the exposition.

Figure 5 shows the computed frequencies, damping and participation factors, plotted for varying rotor speed. Each frequency plot represents a diverging fan, each fan labeled by the classical name of its principal harmonic. Looking at the plots of the participation factors, which correspond to the definition given in (17), it appears here again that both in-plane whirling modes are characterized by a strongly periodic behavior, and their response is not well described by a single frequency.

Notice also from Table III how the dualism 'rotating/fixed frame frequencies' is viewed through the output-specific participation factors. In fact, output ζ_1, which is a rotating frame degree of freedom, has non-negligible super-harmonic participations, especially for the tower, backward and forward whirling modes at $\pm i\Omega$.[18] On the other hand, the fixed frame output y_c is less strongly periodic, and only the principal harmonics appear prominently in its response. In fact, the

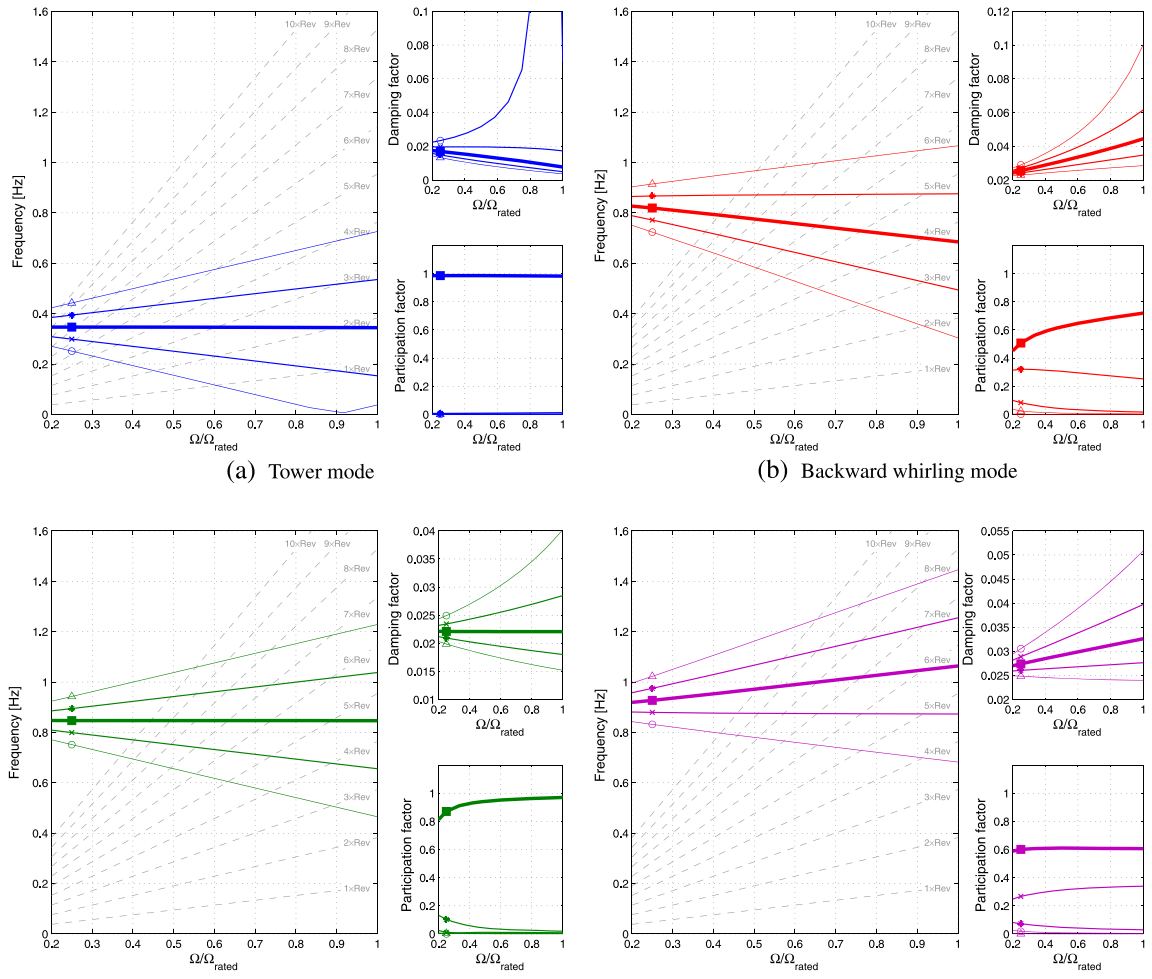

(a) Tower mode (b) Backward whirling mode

(c) Blade edgewise mode (d) Forward whirling mode

Figure 5. Frequencies, damping and participation factors for the rotor-tower model problem, computed at varying rotor speeds.

dominant harmonics for each mode depend on the specific outputs, and thus on the frame of observations, as expressed by equations (19–25); this fact must be considered when analyzing the causes of vibratory phenomena.

Although the present model problem is quite simple, it still captures some interesting effects that help in clarifying the difference between a fully periodic analysis and an MBC-LTI analysis. In fact, the presence of gravity renders the rotor anisotropic, because of variable lag stiffness depending on the blade azimuthal position (cf. matrix $\boldsymbol{K}(\psi)$ in equation (37c)). Hence, Coleman transforming the rotating lag degrees of freedom will not exactly remove periodicity from $\boldsymbol{K}(\psi)$, although it will do so for the mass and damping matrices. Given definition (36) of the coordinate vector, the Coleman transformation matrix is

$$\boldsymbol{B}(\ ) = \begin{bmatrix} 1 & \cos(\psi_1) & \sin(\psi_1) & 0 \\ 1 & \cos(\psi_2) & \sin(\psi_2) & 0 \\ 1 & \cos(\psi_3) & \sin(\psi_3) & 0 \\ 0 & 0 & 0 & 1 \end{bmatrix} \tag{38}$$

and, upon transformation according to $\boldsymbol{K}_{\mathrm{MBC}}(\psi) = \boldsymbol{B}^{-1}(\psi)\boldsymbol{K}(\psi)\boldsymbol{B}(\psi)$, the resulting stiffness is

$$\boldsymbol{K}_{\mathrm{MBC}}(\psi) = \begin{bmatrix} eR\Omega^2 + K_\zeta & \dfrac{g\,S_b}{2} & 0 & 0 \\ g\,S_b & eR\Omega^2 + K_\zeta + \dfrac{g\,S_b}{2}\cos(3\psi_1) & \dfrac{g\,S_b}{2}\sin(3\psi_1) & 0 \\ 0 & \dfrac{g\,S_b}{2}\sin(3\psi_1) & eR\Omega^2 + K_\zeta - \dfrac{g\,S_b}{2}\cos(3\psi_1) & 0 \\ 0 & \dfrac{3}{2}\Omega^2\,S_b & 0 & K_c \end{bmatrix}. \tag{39}$$

As expected, the transformed matrix exhibits a small remaining periodicity at three per-rev because of the presence of gravity. Figure 6 shows the Frobenius norm of the amplitude of the first harmonics of the Lyapunov–Floquet and Coleman transformations. Among the infinite possible Lyapunov–Floquet transformations, we chose the one that is more similar to the Coleman one. To make this possible, one must first generalize equation (6) as $\Phi(t) = \boldsymbol{P}(t)e^{\boldsymbol{R}t}\boldsymbol{P}(0)^{-1}$ by considering a generic invertible initial condition for $\boldsymbol{P}$[14] and then setting $\boldsymbol{P}(0) = \boldsymbol{B}(0)$. The figure shows very clearly that the Coleman transformation approximates well the constant and the one per-rev content of the Lyapunov–Floquet transformation, while it completely neglects all higher frequencies.

The dependence of the Froude number, which measures the relative weight of the aerodynamic and gravitational forces, on the inverse of a characteristic length (e.g., the rotor radius), implies that gravitational effects are expected to

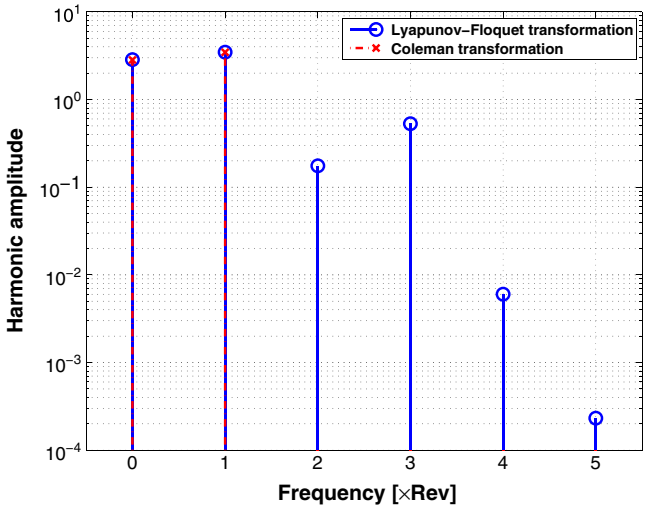

Figure 6. Frobenius norm of the amplitude of the first harmonics of the Lyapunov–Floquet (circles) and of the Coleman (x marks) transformations.

play a prominent role in future very large wind turbines. In turn, this might soon emphasize the limits of the classical Coleman-based analysis.

3. SYSTEM IDENTIFICATION OF LTP SYSTEMS FROM INPUT–OUTPUT DATA

In the previous section, it was shown how to conduct a rigorous stability analysis of LTP systems. In this section, we show how to build a discrete-time state-space LTP model from a sequence of N measurements, restricting the discussion to the single-input/single-output open-loop case. This result is obtained in two steps: first, a PARX input–output model is identified, which is then realized in state-space form to yield the final discrete-time model used for stability analysis.

The equation-error method was used by Bertogalli *et al.*[19] for the identification of a periodic model of a helicopter rotor; this approach leads to the solution of a least-squares problem. On the other hand, the output-error method[20,21] allows one to consider the presence of measurement noise but necessitates a non-linear iteration for its solution. Conceptually, both the equation and output-error methods aim at describing the dynamics of an input/output sequence. However, the different treatments of measurement noise implies that models identified with the output-error approach typically better capture the dynamics of the system that generated the data.[20] Because of this, in this work, we adopt the output-error method for its superior statistical characteristics. However, to ease its convergence, we use the equation-error method to generate a suitable initial guess for the non-linear solution. Both methods are briefly reviewed in the following in the context of the present PARX identification problem.

3.1. Equation-error identification of LTP systems

In the equation-error approach, output samples $z(k)$, $k = 1, \ldots, N$, are assumed to obey the following PARX sequence:

$$z(k) = \sum_{i=1}^{N_a} a_i(k) z(k-i) + \sum_{j=0}^{N_b} b_j(k) u(k-j) + r(k) \tag{40}$$

where $a_i(k) = a_i(k+K)$ are the N_a unknown periodic coefficients of the autoregressive part, $b_j(k) = b_j(k+K)$ the N_b unknown periodic coefficients of the exogenous part, while $r(k)$ is the Gaussian and white equation error. These assumptions on the characteristics of the error might be violated in general because of unmodeled dynamics or measurement biases.

To reduce the number of unknowns, the periodic coefficients $a_i(k)$ and $b_j(k)$ can be approximated by using truncated Fourier expansions, i.e.,

$$a_i(k) = a_{i0} + \sum_{l=1}^{N_{Fa}} \left(a_{il}^c \cos\left(l\psi(k)\right) + a_{il}^s \sin(l\psi(k)) \right) \tag{41a}$$

$$b_j(k) = b_{j0} + \sum_{m=1}^{N_{Fb}} \left(b_{jm}^c \cos\left(m\psi(k)\right) + b_{jm}^s \sin(m\psi(k)) \right). \tag{41b}$$

The unknown coefficients a_{i0}, a_{il}^c, a_{il}^s, b_{j0}, b_{jm}^c and b_{jm}^s are collected in a vector of parameters $\boldsymbol{p}$ to be identified:

$$\boldsymbol{p} = \left(\ldots, a_{i0}, a_{il}^c, a_{il}^s, \ldots, b_{j0}, b_{jm}^c, b_{jm}^s, \ldots \right)^T \tag{42}$$

where $i = (1, \ldots, N_a)$, $j = (1, \ldots, N_b)$, $l = (1, \ldots, N_{F_a})$ and $m = (1, \ldots, N_{F_b})$.

Define now the row vectors

$$\boldsymbol{\varphi}_a\left(\psi(k)\right) = \left[1, \cos\left(\psi(k)\right), \ldots, \cos\left(N_{Fa}\psi(k)\right), \sin\left(\psi(k)\right), \ldots, \sin\left(N_{Fa}\psi(k)\right)\right] \tag{43a}$$

$$\boldsymbol{\varphi}_b\left(\psi(k)\right) = \left[1, \cos\left(\psi(k)\right), \ldots, \cos\left(N_{Fb}\psi(k)\right), \sin\left(\psi(k)\right), \ldots, \sin\left(N_{Fb}\psi(k)\right)\right] \tag{43b}$$

and in turn

$$\boldsymbol{a}_{r,s} = z(r)\boldsymbol{\varphi}_a\left(\psi(s)\right) \tag{44a}$$

$$\boldsymbol{b}_{r,s} = u(r)\boldsymbol{\varphi}_b\left(\psi(s)\right). \tag{44b}$$

By writing equation (40) for all recorded output signals, one obtains the following overdetermined system

$$\begin{Bmatrix} z(n) \\ z(n+1) \\ \vdots \\ z(N) \end{Bmatrix} = \begin{bmatrix} \boldsymbol{a}_{n-1,n} & \dots & \boldsymbol{a}_{n-N_a,n} & \boldsymbol{b}_{n,n} & \dots & \boldsymbol{b}_{n-N_b,n} \\ \boldsymbol{a}_{n,n+1} & \dots & \boldsymbol{a}_{n-N_a+1,n+1} & \boldsymbol{b}_{n+1,n+1} & \dots & \boldsymbol{b}_{n-N_b+1,n+1} \\ \vdots & \vdots & \vdots & \vdots & \vdots & \vdots \\ \boldsymbol{a}_{N-1,N} & \dots & \boldsymbol{a}_{N-N_a,N} & \boldsymbol{b}_{N,N} & \dots & \boldsymbol{b}_{N-N_b,N} \end{bmatrix} \boldsymbol{p} \tag{45}$$

where $n = \max(N_a, N_b) + 1$. The unknown vector of parameters $\boldsymbol{p}$ is then readily obtained by a least-squares solution of equation (45).

3.2. Output-error identification of LTP systems

In the output-error approach, it is assumed that an error-free output signal $y(k)$ obeys a PARX sequence

$$y(k) = \sum_{i=1}^{N_a} a_i(k) y(k-i) + \sum_{j=0}^{N_b} b_j(k) u(k-j) \tag{46}$$

whereas an error $r(k)$ affects measurements $z(k)$, i.e.,

$$z(k) = y(k) + r(k). \tag{47}$$

As in the previous case, coefficients $a_i(k)$ and $b_j(k)$ are approximated with a suitable number of harmonics using (41).

The resulting unknown vector of parameters $\boldsymbol{p}$ is computed by minimizing a quadratic cost function defined as the sum of the square of the output error:

$$J = \frac{1}{2} \sum_{k=1}^{N} (z(k) - \hat{y}(k; \boldsymbol{p}))^2 \tag{48}$$

where $\hat{y}(k; \boldsymbol{p})$ indicates the prediction of $y(k)$ for a given set of parameters, computed by solving (46) for $k = \max(N_a, N_b) + 1, \dots, N$ starting from initial conditions chosen such that $\hat{y}(k; \boldsymbol{p}) = z(k)$ for $k = 1, \dots, \max(N_a, N_b)$. Minimization of J involves a non-linear iteration because the sensitivity $\partial \hat{y}(k; \boldsymbol{p}) / \partial \boldsymbol{p}$, needed to perform the optimization, depends on the past values of $\hat{y}(k; \boldsymbol{p})$, which in turn depends on the parameters.

3.3. Realization of the PARX sequence in state-space form

Once the PARX coefficients are computed, a periodic realization in state-space form is necessary in order to perform the stability analysis as previously described. To this end, consider a discrete-time state-space system in observable canonical form

$$\boldsymbol{x}(k+1) = \boldsymbol{A}(k)\boldsymbol{x}(k) + \boldsymbol{B}(k)u(k) \tag{49a}$$

$$y(k) = \boldsymbol{C}(k)\boldsymbol{x}(k) + \boldsymbol{D}(k)u(k) \tag{49b}$$

where

$$\left[\begin{array}{c|c} \boldsymbol{A}(k) & \boldsymbol{B}(k) \\ \hline \boldsymbol{C}(k) & \boldsymbol{D}(k) \end{array}\right] = \left[\begin{array}{ccccc|c} 0 & 0 & \dots & 0 & \alpha_n(k) & \beta_n(k) \\ 1 & 0 & \dots & 0 & \alpha_{n-1}(k) & \beta_{n-1}(k) \\ 0 & 1 & \dots & 0 & \alpha_{n-2}(k) & \beta_{n-2}(k) \\ \vdots & \ddots & \ddots & \vdots & \vdots & \vdots \\ 0 & 0 & \dots & 1 & \alpha_1(k) & \beta_1(k) \\ \hline 0 & 0 & \dots & 0 & 1 & \beta_0(k) \end{array}\right]. \tag{50}$$

Considering the nth component of $\boldsymbol{x}(k)$, labeled $x_n(k)$, the following sequence is derived from (49a) and (50):

$$x_n(k) = x_{n-1} + \alpha_1(k-1)x_n(k-1) + \beta_1(k-1)u(k-1) \tag{51a}$$

$$= x_{n-2}(k-2) + \alpha_2(k-2)x_n(k-2) + \alpha_1(k-1)x_n(k-1) + \beta_1(k-1)u(k-1) + \beta_2(k-2)u(k-2) \tag{51b}$$

$$= \dots \tag{51c}$$

$$= \sum_{i=1}^{n} \alpha_i(k-i)x_n(k-i) + \sum_{i=1}^{n} \beta_i(k-i)u(k-1). \tag{51d}$$

Considering now the output equation (49b), we have

$$y(k) = x_n(k) + \beta_0(k)u(k) \tag{52}$$

which readily yields the system input–output sequence:

$$y(k) = \sum_{i=1}^{n} \alpha_i(k-i)y(k-i) + \sum_{i=1}^{n} \big[\beta_i(k-i) - \beta_0(k-i)\alpha_i(k-i)\big]u(k-i) + \beta_0(k)u(k). \tag{53}$$

Comparing (53) with (40), it can be easily shown that (49–50) is equivalent, i.e., it has the same impulsive response, to (40) if the system coefficients are chosen as follows:

$$\alpha_j(k) = a_j(k+j), \quad \forall j = (1, \dots, N_a) \tag{54a}$$

$$\beta_0(k) = b_0(k) \tag{54b}$$

$$\beta_j(k) = b_j(k+j) + a_j(k+j)b_0(k), \quad \forall j = (1, \dots, N_b). \tag{54c}$$

4. RESULTS

A detailed aero-elastic model of a direct-drive 6 MW wind turbine was used in this work for testing the proposed stability analysis formulation. The model, implemented with the wind turbine simulation code `Cp-Lambda`,[27,28] is based on a finite element multibody approach, using Cartesian coordinates and scaled Lagrange multipliers for the enforcement of constraints. Time marching is performed with an implicit non-linearly unconditionally stable energy decaying scheme. In the following examples, the time step length was kept fixed for each simulation and chosen to ensure an azimuthal swept angle within each step of about 3°. Blades and tower are modeled with geometrically exact beam elements, while aerodynamics is rendered by a classical blade-element momentum (BEM) model based on the annular stream-tube theory with wake swirl, including tip and hub loss models, including unsteady corrections and dynamic stall. The resulting total number of degrees of freedom in the model is slightly greater than 2500. The model is complemented by a pitch–torque control system.

The following examples consider only the open-loop case. Consequently, after having trimmed the machine at the desired set points, all control inputs were kept fixed to their trim values during and after the excitation phase. The stability analysis method described herein could be extended to closed-loop systems. To this end, care must be exercised to ensure the effectiveness of the closed-loop identification process (cf., for example, the work of van der Veen *et al.*,[29] Iribas and Landau[30] and Van den Hof[31]).

While the implementation of an MBC-LTI approach in a code of similar complexity would be a major undertaking, we stress here again that the use of a different simulation tool other than `Cp-Lambda` would require no change to the software implementation of the proposed stability analysis procedures.

4.1. Rotor edgewise response

At first, we consider the estimation of the level of damping of the edgewise rotor modes, which is typically quite light because of the small aerodynamic damping associated with such motions. In order to perturb the system, two edgewise force doublets were applied near the blade tip and at mid-span. Amplitude and length of the doublets were tuned so as to excite a linear response of the modes of interest. This was verified by perturbing the system with forces of different amplitude and checking if the peaks related to the modes of interest were actually in a linear proportion to the perturbation intensity. The analysis was conducted in constant non-turbulent wind conditions at 15 m s^{-1}, between rated rotor speed Ω_r and 1.33 Ω_r, so as to investigate the behavior of the system in the over-speed regime. The pitch angle was kept frozen to the

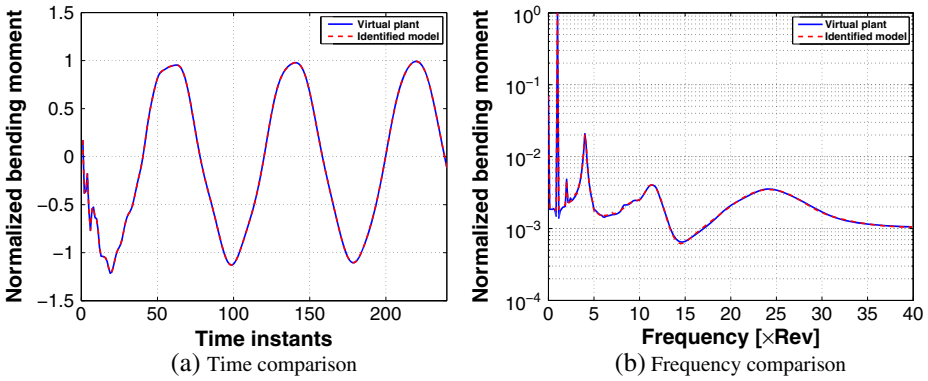

(a) Time comparison (b) Frequency comparison

Figure 7. Comparison between measured (solid line) and predicted (dashed line) normalized blade root bending moment, in the time (left) and frequency (right) domains.

Table IV. First and second blade edgewise fans of modes.

Frequency [×Rev]	Damping	Participation
(a) 1st blade edgewise mode		
2.0321	0.0434	0.0114
3.0314	0.0291	0.1351
4.0311	0.0219	0.5807
5.0309	0.0175	0.1392
6.0308	0.0146	0.0013
(b) 2nd blade edgewise mode		
9.2661	0.1137	0.0344
10.2602	0.1027	0.1839
11.2554	0.0936	0.4173
12.2514	0.0860	0.2112
13.2479	0.0796	0.0754

values corresponding to the rated rotor speed condition, whereas the trim at over-speed regimes was obtained by adjusting the torque with a simple PD controller.

The order of the to-be-identified reduced model was chosen according to some simple considerations. First, since the frequency content of the outputs shows three distinct peaks (Figure 7(b)), N_a was set equal to 6. Second, the fact that the wind is constant allows one to identify only coefficient $\beta_1(k)$ of the exogenous part of the model, so that $N_b = 1$. Furthermore, by trial and error, the periodicity of the coefficients was approximated with $N_{F_a} = 1$ and $N_{F_b} = 6$. Small oscillations (of the order of 1%) of the rotor speed were removed by averaging over a few revolutions; given the small size of such oscillations, considering the rotor speed as constant appears to be a completely acceptable approximation.

Figure 7 shows a comparison between the normalized edgewise root bending moment that was measured on the simulation model (solid line) and the one predicted by the identified PARX one (dashed line), in the time (left) and frequency (right) domains, for a rotor speed equal to about 1.13 Ω_r. The plots show an excellent correlation between the quantities of the virtual plant and of the identified model. Notice that the third mode has a very short characteristic time, such that it vanishes very quickly in the first time instants after perturbation; this is also the span of time used to compute the initial conditions. This implies that results related to the third mode do not have the same level of accuracy of the first and second modes. For this same operating condition, Table IV reports the frequency, damping and participation factors of the lowest five harmonics for the first and second edgewise fans of modes.

Figure 8 shows, for the lowest edgewise fan, the normalized frequencies (scaled by the rated rotor speed), damping and participation factors as functions of rotor speed. Note the rough behavior of the participation factors, because uncertainties propagate more in these quantities than in frequencies or damping factors.

The periodic Campbell diagram of Figure 8 at the left shows resonant conditions around a rotor speed of 1.15 Ω_r. In fact, not only the principal frequency with the highest participation intersects the four per-rev but also the other super-harmonics intersect different per-rev excitation harmonics. These multiple resonances are not just a curious side effect of a fully periodic stability analysis but are indeed visible in the machine response. In fact, based on the suggestion given by Figure 8, by looking carefully at the behavior of the system, one can recognize the presence of multiple mild resonances appearing

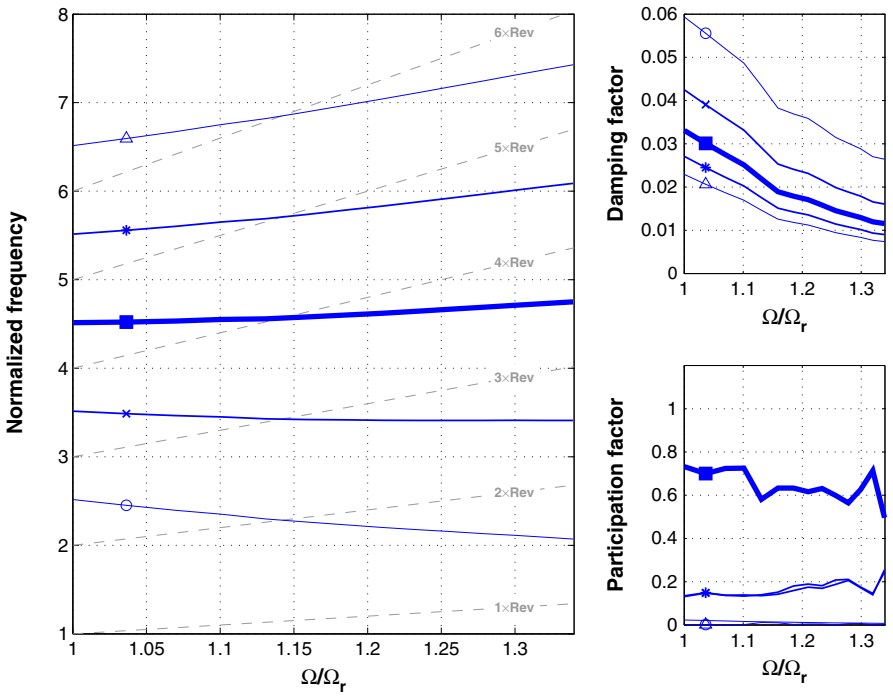

Figure 8. Frequencies, damping and participation factors of the first edgewise mode.

around 1.15 Ω_r. Figure 9 shows the amplitude of the harmonics of the blade root edgewise bending moment, computed in a stationary trimmed condition in constant wind, as a function of rotor speed. Notice, apart from the four per-rev resonance, also the presence of other peaks at two, five and six per-rev, as predicted by the periodic Campbell diagram. Here again, the presence of these peaks could not be justified if the mode was described by a single frequency.

4.2. Tower side–side response

A zero-mean side–side force chirp applied at the tower top was used to perturb the machine operating in open-loop under the effects of a steady mean wind. The time history of the blade root edgewise bending moment and tower base fore-aft and side–side bending moments were recorded from the end of the perturbing signal. In this case, N_a was set equal to 2 in order to model the presence of a single mode, and since the wind remains constant, N_b was set to 1, while the Fourier truncation of the coefficients was performed with $N_{F_a} = N_{F_b} = 5$.

Figure 10 shows a comparison between the virtual plant measurement and the identified output in the frequency domain, for the tower side–side bending moment at a wind speed of 5 m s^{-1}. Table V summarizes the results in terms of frequency, damping and participation factors for the first tower side–side fan of modes. Even if the principal tower frequency around 2.8 per-rev has a participation that is close to 1, its associated super-harmonics are visible in the Fourier transform of the response displayed in Figure 10.

The simplified model problem discussed previously showed that the tower super-harmonics may appear prominently in the blade response. To verify this fact with respect to the present more realistic case, we performed the identification of a new model using the blade root edgewise bending moment measurements. Figure 11 and Table VI summarize the results. As expected from the model problem, even here, the figure shows two prominent peaks related to the tower super-harmonics. Notice also, as a side note, the presence of a small peak at a frequency of about 10 per-rev, which is one super-harmonic of the forward in-plane whirling fan, similar to what can be observed for the simplified model problem in Figure 4(a).

Table VI(a) shows that, although the tower principal harmonic is not visible in the response (cf. Figure 11), its frequency is still correctly estimated (cf. the present value of 2.7955 with the one in Table V of 2.7935). The periodic identification is capable of assigning the two peaks related to the tower super-harmonics to a single mode fan, both having high participation factors, while a participation close to 0 is assigned to the principal harmonic.

Comparing Tables V and VI(a), one can again observe the phenomenon previously illustrated with the help of the simplified model problem: the first tower side–side fan of modes has a markedly invariant character when observed through the tower response (the tower base bending in this case), while a strongly periodic one when observed through the blade

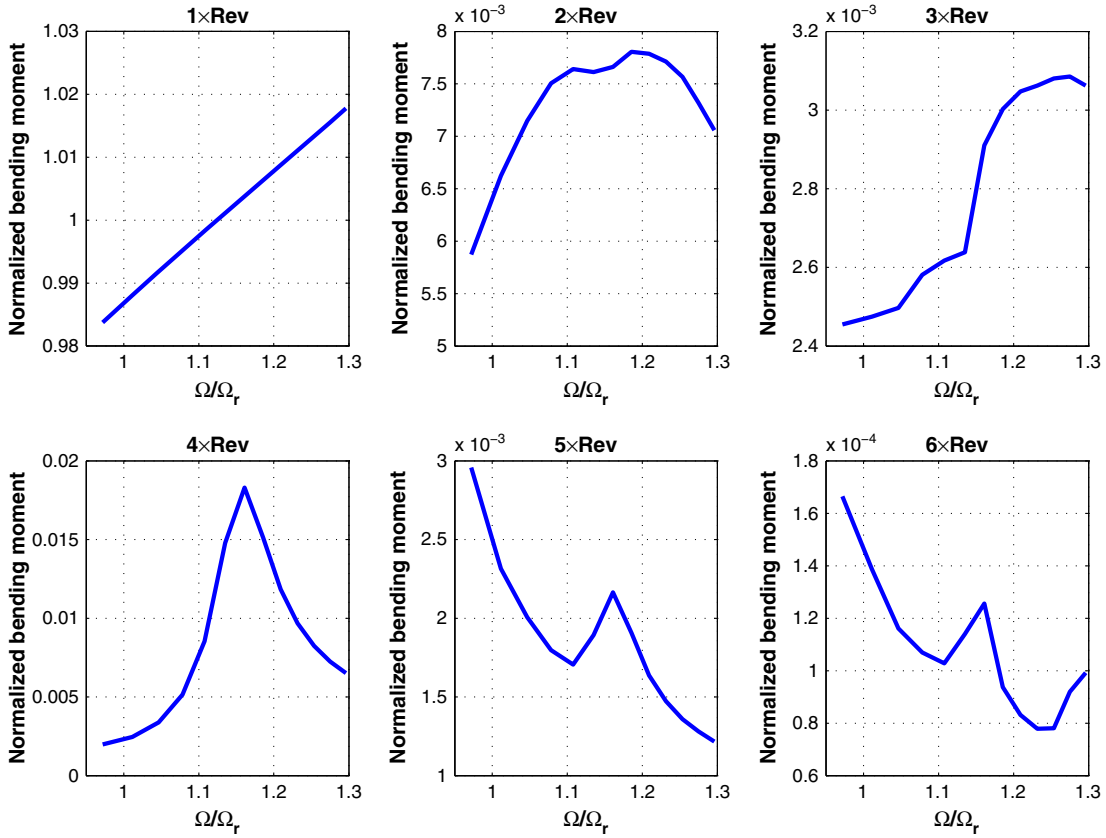

Figure 9. Amplitude of the one to six per-rev edgewise blade root moment harmonics as a function of rotor speed. Values are scaled with the maximum edgewise moment at Ω_r.

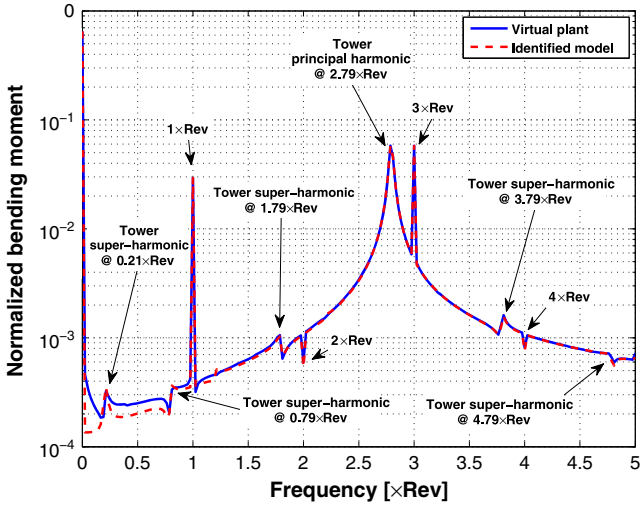

Figure 10. Comparison between measured (solid line) and predicted (dashed line) normalized tower base side–side bending moment in the frequency domain.

Table V. First tower side–side fan of modes.

Frequency [×Rev]	Damping	Participation
0.2072	0.0783	0.007
0.7936	0.0204	0.004
1.7935	0.0090	0.006
2.7935	0.0058	0.964
3.7935	0.0043	0.009
4.7935	0.0034	0.002

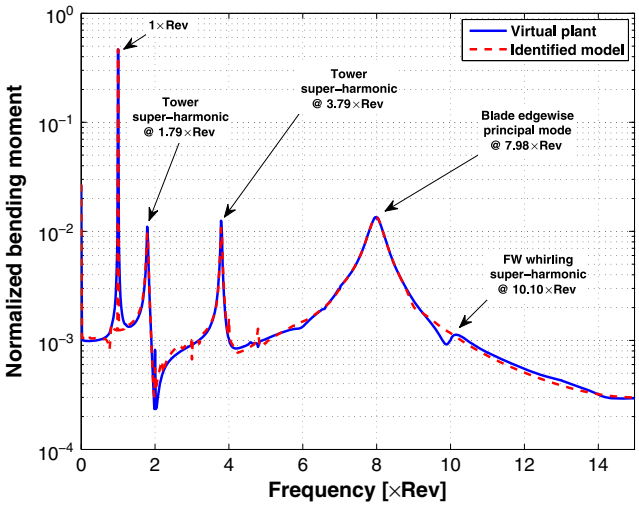

Figure 11. Comparison between measured (solid line) and predicted (dashed line) normalized blade root edgewise bending moment in the frequency domain.

Table VI. Side–side tower and blade edgewise fans of modes.

Frequency [×Rev]	Damping	Participation
(a) 1st tower side–side mode		
0.7957	0.0283	0.0243
1.7955	0.0125	0.3557
2.7955	0.0080	0.0901
3.7955	0.0059	0.4319
4.7954	0.0047	0.0685
(b) 1st blade edgewise mode		
5.9900	0.0343	0.0015
6.9895	0.0294	0.0899
7.9891	0.0257	0.7872
8.9888	0.0229	0.0985
9.9885	0.0206	0.0021

response (the blade edgewise bending in this case), coherently with physical intuition. We further note that, because of the definition of the output in the realized state-space model of equations (49) and (50), modal participation factors computed from the identification and realization of a PARX model are automatically output specific.

4.3. Tower fore-aft and in-plane whirling response

Because of the coupling between fore-aft and side–side tower modes, the backward and forward in-plane whirling modes are visible in both the fore-aft and side–side tower base moments. In this work, the in-plane whirling modes were identified

from the fore-aft moment, since the response in the side–side direction is dominated by the very low-damped side–side tower mode.

The two backward and forward whirling modes are separated in frequency by about 2 Ω. This fact may have an effect on the identification process, because different modes separated by multiples of the rotor frequency could be interpreted as different super-harmonics of the same fan of modes. To overcome this issue, an invariant model, obtained by simply setting $N_{Fa} = 0$, was fitted to the measurements. The resulting model, which necessarily considers the backward and forward whirlings as two distinct modes since it is blind to the presence of fans, was then used as the initial guess for the identification of the periodic model.

Results of the identification conducted in this way are shown for a uniform wind condition at 5 m s^{-1} in Figure 12 and Table VII. The identified model matches well the response of the system, although there are minor spurious oscillations, which determine the unexpected high participation of the $+2\Omega$ super-harmonic of the backward whirling mode.

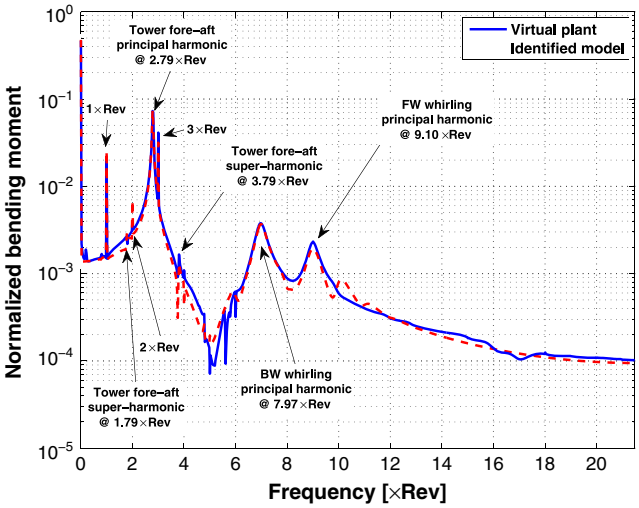

Figure 12. Comparison between measured (solid line) and predicted (dashed line) normalized tower base fore-aft bending moment in the frequency domain.

Table VII. First tower fore-aft and in-plane whirling fans of modes.

Freq [×Rev]	Damping	Participation
(a) 1st tower fore-aft mode		
0.7858	0.0268	0.0008
1.7856	0.0118	0.0675
2.7856	0.0075	0.8691
3.7855	0.0056	0.0607
4.7855	0.0044	0.0014
(b) Backward in-plane whirling		
4.9760	0.0394	0.0034
5.9754	0.0328	0.0541
6.9749	0.0281	0.5624
7.9746	0.0246	0.1178
8.9743	0.0218	0.1899
(c) Forward in-plane whirling		
7.1021	0.0336	0.0583
8.1016	0.0295	0.1577
9.1012	0.0262	0.5758
10.1009	0.0236	0.1651
11.1007	0.0215	0.0306

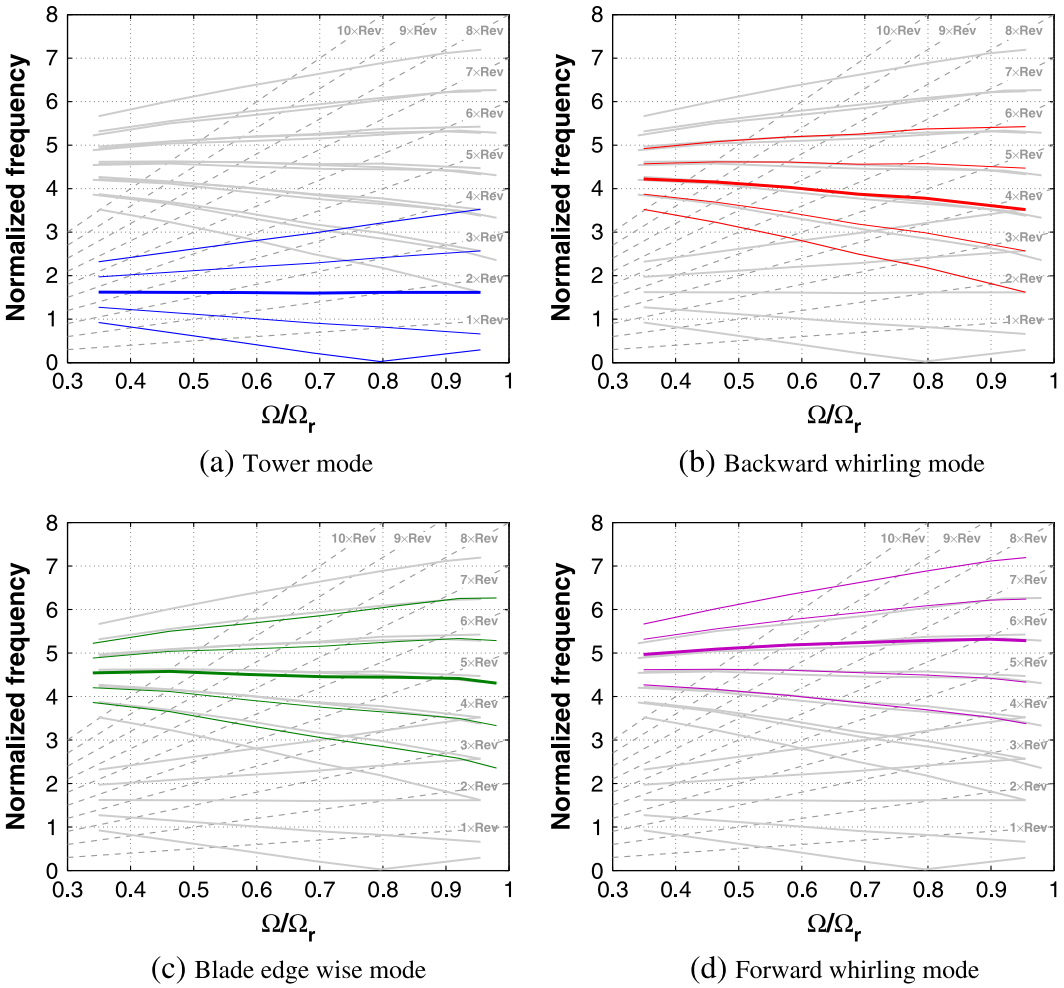

Figure 13. Periodic Campbell diagram by fans of modes (not a complete representation of all lower fans).

4.4. The periodic Campbell diagram

The previously identified fans of modes, computed from the minimum to the rated rotor speed, are collected in the partial periodic Campbell diagram shown in Figure 13. The figure shows the principal harmonic (thick solid line) and four super-harmonics (thin solid lines) for the first tower fore-aft, backward in-plane whirling, blade edgewise and forward in-plane whirling fans of modes. The per-rev excitation harmonics are reported as gray dashed lines emanating from the origin of the plot. For better readability, the plot is repeated four times, one for each fan of modes. Each plot reports in color solid lines the harmonics of one specific fan. A complete Campbell diagram should also report other relevant fans of modes, as the first tower side–side, blade flap, out-of-plane whirling modes, etc., which, however, were not reported here for the sake of simplicity.

This plot should highlight once again that the full picture of the possible resonant conditions emerging from a periodic analysis is much richer than the one obtained by classical means. This scenario is further complicated by the fact that the same harmonic can have a high or low participation factor depending on the specific output considered, something that is difficult to synthesize in one single diagram as the one shown here.

5. CONCLUSIONS

In this work, we have presented a new method for the stability analysis of wind turbines, that is based on the identification of an LTP reduced model that best fits a transient response of the system. Once the model has been identified, stability is assessed using the theory of Floquet for periodic systems.

Based on the simulation results shown earlier in this paper, the following considerations can be drawn:

- The proposed method, since it operates on the basis of input–output sequences, is applicable to models of arbitrary complexity as well as to arbitrary systems (wind turbines, helicopters, etc.).
- Floquet theory shows that a single frequency is not sufficient to fully characterize a periodic mode, because in reality several multi-harmonics participate in the response of the system and each of them may resonate with the per-rev excitations. The presence of these additional harmonics, which was shown to appear in the spectra of simplified model problems as well as more realistic wind turbine models, cannot be explained by the widespread simplified time-invariant approaches, for which only one frequency is associated to each mode. In the ideal case of an isotropic rotor, the MBC-LTI approach provides the same results of the Floquet analysis, and in the more realistic cases, it yields three harmonics for each mode. While this is typically more than appropriate, unfortunately, it is difficult to quantify *a priori* the level of approximation of such method without performing a full Floquet analysis, and more research needs to be carried out to understand the condition for which the approximations of the MBC-LTI method are acceptable, and when they are not.
- The use of the participation factor allows one to measure how periodically (or invariantly) a specific fan behaves. This concept also clarifies the issue of the apparent indetermination of characteristic exponents, which was a major source of confusion in the literature in the (vain) attempt to characterize a periodic mode with a single frequency.
- For the examples studied herein, it was always possible to identify reduced models of excellent quality, i.e., that produced outputs very close to the measured ones. For other common problems in system identification, one has to guarantee the generality of the identified model, i.e., its ability to approximate also situations that are not in the identification data set. In the present application, this is not necessary, and this greatly simplifies the problem of obtaining good quality reduced models, which in turn helps in achieving good quality results from the stability analysis.

The present study can be improved and expanded in a few directions.

In terms of improvements, the most important one might be the use of multiple outputs, as opposed to the single output used here. In fact, it was shown how super-harmonics could manifest themselves in different ways for different signals, as shown by the case of the tower super-harmonics that were inconspicuous in the tower loads but showed prominently in the blade ones. Furthermore, this means that one has to identify different models for different modes and has to pick the best signal for each, which complicates the process. The use of multiple outputs in the identification process could significantly simplify this aspect.

In terms of expansions of the proposed approach, the most obvious one is the application to real wind turbines operating in the field. This could be carried out by using, instead of the PARX model used here, a PARMAX (Periodic Auto-Regressive Moving Average with eXogeneous input) one, so as to include the effects of wind turbulence as a process noise term, possibly through the use of a suitable turbulence model to avoid assuming whiteness. Moreover, one should consider the effects on the estimation procedure of a closed-loop controller, as well as of possible large variations of the rotor speed due to turbulence. This could lead to the investigation of different estimation techniques, which may range from subspace[32,33] to frequency domain methods,[23] or different input–output models, such as the Box–Jenkins, ARARMAX or pseudo-linear regression models.[20] All these issues are currently under investigation.

ACKNOWLEDGEMENT

The present research was in part funded by the EU FP7 project INNWIND, whose support is gratefully acknowledged.

REFERENCES

1. Bialasiewicz JT, Richard MO, Advanced system identification techniques for wind turbine structures. *NREL/TP-442-6930*, 1995.
2. Hansen MOL, Sørensen JN, Voutsinas S, Sørensen N, Madsen HAa. State of the art in wind turbine aerodynamics and aeroelasticity. *Progress in Aerospace Sciences* 2006; **42**: 285–330.
3. Hansen MH, Thomsen K, Fuglsang P. Two methods for estimating aeroelastic damping of operational wind turbine modes from experiments. *Wind Energy* 2006; **9**: 179–191.
4. Chauhan S, Hansen MH, Tcherniak D. Application of operational modal analysis and blind source separation/indipendent component analysis techniques to wind turbines. *Proceedings of 27th IMAC Conference*, Orlando, Florida, February 9–12, 2009.
5. Balaguer I, Kanev S, Tcherniak D, Rossetti M. System identification methods on Alstom ECO 100 wind turbine. *Proceedings of 3rd Torque Conference*, Heraklion, Crete, Greece, June 28–30, 2010.
6. Eggleston DM, Stoddard FS. *Wind Turbine Engineering Design*. Van Nostrand Reinhold: New York, NY, USA, 1987.

7. Floquet G. Sur les équations différentielles linéaires à coefficients périodiques. *Annales Scientifiques de l'E.N.S.* 1883; **2**: 47–88.
8. Hansen MH. Aeroelastic stability analysis of wind turbines using an eigenvalue approach. *Wind Energy* 2004; **7**: 133–143.
9. Skjoldan PF, Hansen MH. Implicit Floquet analysis of wind turbines using tangent matrices of a non-linear aeroelastic code. *Wind Energy* 2012; **15**: 275–287.
10. Coleman RP, Feingold AM, Theory of self-excited mechanical oscillations of helicopter rotors with hinged blades. *NACA Report TN 1351*, 1958.
11. Johnson W. *Helicopter Theory*. Princeton University Press: New Jersey, 1980.
12. Bir G. Multi-blade coordinate transformation and its application to wind turbine analysis. *Proceedings of the AIAA Wind Energy Symposium*, Reno, Nevada, January 7–10, 2008.
13. Skjoldan PF, Hansen MH. On the similarity of the Coleman and Lyapunov–Floquet transformation for modal analysis of blade rotor structures. *Journal of Sound and Vibration* 2009; **327**: 424–439.
14. Bittanti S, Colaneri P. *Periodic Systems—Filtering and Control*. Springer-Verlag: London, 2009.
15. Peters DA, Lieb SM, Ahasus LA. Interpretation of Floquet eigenvalues and eigenvectors for periodic systems. *Journal of the American Helicopter Society* 2010; **56**: 032001-1-11.
16. Bottasso CL, Cacciola S. Periodic stability analysis of wind turbines, EWEA 2012 Annual Event, Copenhagen, Denmark, April 16–19, 2012.
17. Hansen MH. Aeroelastic instability problems for wind turbines. *Wind Energy* 2007; **10**: 551–577.
18. Hansen MH. Improved modal dynamics of wind turbines to avoid stall-induced vibrations. *Wind Energy* 2003; **6**: 179–195.
19. Bertogalli V, Bittanti S, Lovera M. Simulation and identification of helicopter rotor dynamics using a general-purpose multibody code. *Journal of the Franklin Institute* 1999; **366**: 783–797.
20. Ljung L. *System Identification—Theory for the User*. Prentice Hall: Englewood Cliffs, NJ, USA, 1999.
21. Klein V, Morelli EA. *Aircraft System Identification—Theory and Practice*. AIAA Education Series: Reston, VA, USA, 2006.
22. Hauer JF, Demeure CJ, Scharf LL. Initial results in Prony analysis of power system response signals. *IEEE Transaction on Power System* 1990; **5**: 80–89.
23. Allen MS, Sracic MW, Chauhan S, Hansen MH. Output-only modal analysis of linear time periodic systems with application to wind turbine simulation data. *Mechanical Systems and Signal Processing* 2011; **25**: 1174–1191.
24. Borri M. Helicopter rotor dynamics by finite element time approximation. *Computers & Mathematics with Applications* 1986; **12A**: 149–160.
25. Franklin GF, Powell JD. *Digital Control of Dynamic Systems* 1st edition. Addison-Wesley Publishing Company: Reading, MA, USA, 1980.
26. Hammond CE. An application of Floquet theory to prediction of mechanical instability. *Journal of the American Helicopter Society* 1974; **19**: 14–23.
27. Bauchau OA, Bottasso CL, Trainelli L. Robust integration schemes for flexible multibody systems. *Computer Methods in Applied Mechanics and Engineering* 2003; **192**: 395–420.
28. Bottasso CL, Croce A. *Cp-Lambda: User's Manual*. Dipartimento di Ingegneria Aerospaziale: Politecnico di Milano, 2006–2012.
29. van der Veen GJ, van Wingerden JW, Fleming PA, Scholbrock AK, Verhaegen M. Global data-driven modeling of wind turbines in the presence of turbulence. *Control Engineering Practice* 2013; **21**: 441–454.
30. Iribas M, Landau I-D. Identification of wind turbines in closed-loop operation in the presence of three-dimensional turbulence wind speed: torque demand to measured generator speed loop. *Wind Energy* 2009; **12**: 660–675.
31. Van den Hof P. Closed loop issues in system identification. *Annual Reviews in Control* 1998; **22**: 173–186.
32. Gebraad PMO, van Wingerden JW, Fleming PA, Wright AD. LPV identification of wind turbine rotor vibrational dynamics using periodic disturbance basis functions. *IEEE Transactions on Control Systems Technology* 2013; **21**: 1183–1190.
33. van der Veen G, van Wingerden JW, Bergamasco M, Lovera M, Verhaegen M. Closed-loop subspace identification methods: an overview. *IET Control Theory & Applications* 2013; **7**: 1339–1358.